

# Gamow-Teller strength in $^{48}\text{Ca}$ and $^{78}\text{Ni}$ with the charge-exchange subtracted second random-phase approximation

D. Gambacurta,<sup>1</sup> M. Grasso,<sup>2</sup> and J. Engel<sup>3</sup>

<sup>1</sup>*INFN-LNS, Laboratori Nazionali del Sud, 95123 Catania, Italy*

<sup>2</sup>*Université Paris-Saclay, CNRS/IN2P3, IJCLab, 91405 Orsay, France*

<sup>3</sup>*Department of Physics and Astronomy, CB 3255,*

*University of North Carolina, Chapel Hill, North Carolina 27599-3255, USA*

We develop a fully self-consistent subtracted second random-phase approximation for charge-exchange processes with Skyrme energy-density functionals. As a first application, we study Gamow-Teller excitations in the doubly-magic nucleus  $^{48}\text{Ca}$ , the lightest double- $\beta$  emitter that could be used in an experiment, and in  $^{78}\text{Ni}$ , the single-beta-decay rate of which is known. The amount of Gamow-Teller strength below 20 or 30 MeV is considerably smaller than in other energy-density-functional calculations and agrees better with experiment in  $^{48}\text{Ca}$ , as does the beta-decay rate in  $^{78}\text{Ni}$ . These important results, obtained without *ad hoc* quenching factors, are due to the presence of two-particle – two-hole configurations. Their density progressively increases with excitation energy, leading to a long high-energy tail in the spectrum, a fact that may have implications for the computation of nuclear matrix elements for neutrinoless double- $\beta$  decay in the same framework.

Charge-exchange (CE) excitations [1, 2] such as the Gamow-Teller (GT) resonance are closely linked to electron capture and  $\beta$  decay, which play important roles in nuclear astrophysics [3, 4]. They also aid the construction of nuclear effective interactions, for which they constrain couplings in the spin-isospin channel. Finally, they are relevant to the nuclear physics that affects neutrinoless double- $\beta$  ( $0\nu\beta\beta$ ) decay, in which two neutrons change into two protons [5–7]. The experimental observation of this rare process would be a breakthrough for fundamental physics; it would mean that neutrinos are Majorana particles and would imply new phenomena beyond the Standard Model that could be related to the matter-antimatter asymmetry in the universe. The rate of  $0\nu\beta\beta$  decay depends on nuclear matrix elements that may only be determined theoretically. At present, predictions for these matrix elements differ from one model to the next by factors of two or three, an amount that is too large to allow the efficient planning and interpretation of experiments.

Any model that hopes to describe double- $\beta$  decay must be able to predict the distribution of GT strength because the GT operator, multiplied by the axial-vector coupling constant  $g_A$ , is the leading contribution to the operator that governs  $\beta$  decay. Recent work [8–10] that correlates calculations of double-GT and  $0\nu\beta\beta$  matrix elements even suggests that one could deduce the latter from double-CE experiments [11, 12]. Most double- $\beta$  emitters that could be used in experiments are still too complex to easily treat from first principles with *ab-initio* methods (though recently, such methods were applied to  $^{48}\text{Ca}$  [13–15], and to  $^{76}\text{Ge}$  and  $^{82}\text{Se}$  [15]). More phenomenological approaches are therefore still important, even necessary [16–26]. However, these theoretical schemes do not correctly describe the available data for GT excitations and  $\beta$ -decay half-lives and must resort to *ad hoc* “quenching factors” to obtain reasonable results for GT strength below 20 or 30 MeV of excitation energy. In Ref. [27], for example, models based on the random-

phase approximation (RPA) overestimate the strength significantly. This kind of over-prediction is usually ascribed to missing physics, for example the  $\Delta$  excitation [28] or complex configurations such as two-particle – two-hole (2p2h) excitations [29–31]. The results in Ref. [27] indicate that higher-order correlations are needed beyond those in the RPA, which is essentially a time-dependent version of mean-field theory.

*Ab-initio* work with operators and currents from chiral effective field theory has recently had some success in explaining the quenching in  $\beta$  decay. Reference [32] showed that correlations omitted from the shell model and from mean-field-based calculations, together with two-body weak currents, account for most of that quenching. Reference [33] showed that the same effects quench the integrated  $\beta$  strength function. But weak two-body currents play no obvious role in charge-exchange transitions, and so the implications of this last result for our work are not clear. Similarly, starting from realistic potentials, the authors of Ref. [34] used many-body perturbation theory to derive effective shell-model operators that implicitly include correlations from outside shell-model spaces, obtaining the correct quenching of GT strength in several nuclei of interest for double- $\beta$  experiments, but failing to do so in the lightest of these,  $^{48}\text{Ca}$ . They also had difficulty in that nucleus with two-neutrino double- $\beta$  decay, a very closely related process.

Finally, EDF-based models that go beyond mean-field theory have been proposed for CE excitations, for example in both relativistic (see Refs. [35, 36] for the most recent developments) and nonrelativistic (see for instance Ref. [37]) particle-vibration-coupling models. The predicted integrated strengths are always better than in the (Q)RPA. Again, however, the improvement is minor for  $^{48}\text{Ca}$ . Reference [37] shows that the GT strength below 20 MeV continues to be significantly overestimated in that nucleus, even when beyond-mean-field correlations are included. In this paper a better description of the  $\text{GT}^-$  strength — measured in charge-exchange reactions

by adding a proton and removing a neutron — in  $^{48}\text{Ca}$ , and of the GT  $\beta$  decay of  $^{78}\text{Ni}$ , are achieved with a subtracted second RPA (SSRPA).

Many-body theorists employ RPA-based schemes extensively in atomic, solid-state, and nuclear physics, as well as in quantum chemistry. Extensions are useful wherever beyond-mean-field correlations play an important role. Second RPA, which includes 2p2h configurations for a richer description of the fragmentation and widths of excited states, has thus made its way from nuclear physics, where it was born, to mesoscopic physics [38] and chemistry [39].

Versions of the RPA for CE processes were introduced several decades ago; references [40–42] contain useful discussions of the stability of the Hartree-Fock solution with respect to isospin excitations. The non-trivial step of constructing a full CE second RPA was taken in later, in Ref. [30]. There, one can find expressions for the Hamiltonian matrix, which contains a 1p1h sector characterized by the matrices called  $A_{11}$  and  $B_{11}$ , a sector that mixes 1p1h and 2p2h configurations, with the matrices  $A_{12}$  and  $B_{12}$ , and a pure 2p2h sector, with the matrices  $A_{22}$  and  $B_{22}$ . Because the diagonalization of large dense matrices was impossible at that time, the Hamiltonian matrix was drastically simplified by neglecting the interaction among 2p2h configurations. That step allowed the full SRPA diagonalization to be replaced by an RPA-type computation with an energy-dependent Hamiltonian. Much more recently, a self-energy subtraction procedure was designed for extensions of RPA [43] and implemented in charge-conserving second RPA [44–49] to make the treatment of excitations consistent with ground-state density-functional theory, guarantee Thouless stability, and eliminate ultra-violet divergences.

The CE second RPA developed here is the first that is fully self consistent and includes a subtraction procedure that, just as in the charge-conserving case, corrects the response to make it consistent with ground-state density-functional theory at zero frequency. We apply it in together with the Skyrme interaction [50–52] SGII [53, 54]. The subtraction procedure requires the inversion of the large matrix  $A_{22}$ . To make the problem tractable, we consistently cut off 2p2h configurations at 40 MeV, both in the diagonalization of  $A_{22}$  and its inversion, having verified that results do not change significantly when the cutoff is raised beyond that level.

GT strength is constrained by the Ikeda sum rule, which relates the integrated strengths  $S$  to the number of neutrons  $N$  and protons  $Z$  in the nucleus:

$$S_{GT^-} - S_{GT^+} = 3(N - Z). \quad (1)$$

The sum rule is model independent under the condition of completeness of states and given the properties of isospin operators. It holds in RPA approaches and their extensions if, as in this work, the quasiboson approximation applies.

In nuclei with a significant neutron excess, such as  $^{48}\text{Ca}$  and  $^{78}\text{Ni}$ , the GT $^-$  strength is much larger than GT $^+$

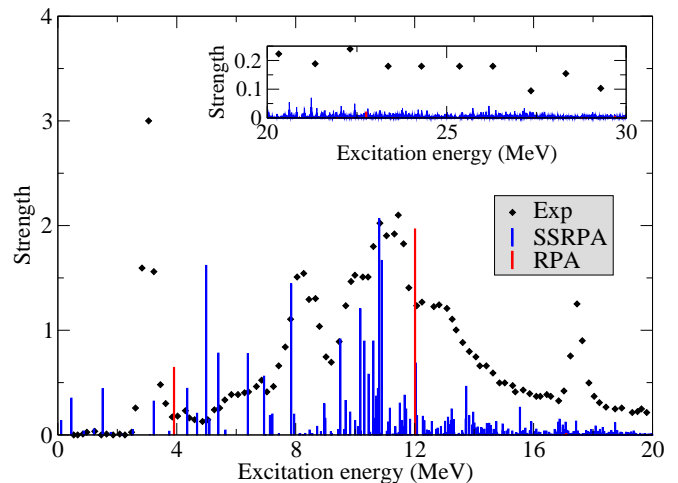


Figure 1. Experimental GT $^-$  plus isovector spin-monopole strength in MeV $^{-1}$  [55] and discrete RPA and SSRPA strength distributions (no units) obtained with the Skyrme parameterization SGII, for  $^{48}\text{Ca}$ . The RPA strength has been divided by nine and the SSRPA strength by two so that the discrete distributions can be displayed on the same figure as the continuous experimental distribution (see text). The insert shows the energy region between 20 and 30 MeV.

strength, measured by adding a neutron and removing a proton. The excitation operator for GT $^-$  transitions can be written as

$$\hat{O}^- = \sum_{i=1}^A \sum_{\mu} \sigma_{\mu}(i) \tau^{-}(i) \quad (2)$$

where  $A$  is the number of nucleons,  $\tau^{-}(i)$  is the isospin-lowering operator  $\tau^{-} \equiv t_x - it_y$  for the  $i^{\text{th}}$  nucleon, and  $\sigma_{\mu}(i)$  is the corresponding spin operator. Because  $S_{GT^-}$  is so much larger than  $S_{GT^+}$  the Ikeda sum rule is essentially a measure of the total GT $^-$  strength (as we will see later numerically).

We begin with the case of  $^{48}\text{Ca}$ . Reference [55] reports the results of a  $^{48}\text{Ca}(p, n)$  and  $^{48}\text{Ti}(n, p)$  experiments at a beam energy of 300 MeV at the Research Center for Nuclear Physics in Osaka. The total GT $^-$  strength below 30 MeV (which probably includes some contributions from isovector spin-monopole excitations) is only  $64 \pm 9\%$  of that given by the Ikeda sum rule. The location of this “missing strength” has long been a mystery for nuclear physics.

Compared to other EDF approaches (both mean-field and beyond-mean-field) ours better predicts the strength distributions, so that we obtain a much more accurate value for the sum of the strength up to 20 or 30 MeV, without resorting to quenching factors. The 2p2h configurations, which increase in density with excitation energy, lead to a long high-energy tail that draws strength from lower energies. The “missing strength” is thus spread out over a large range at higher energies, making it hard to discriminate from background.

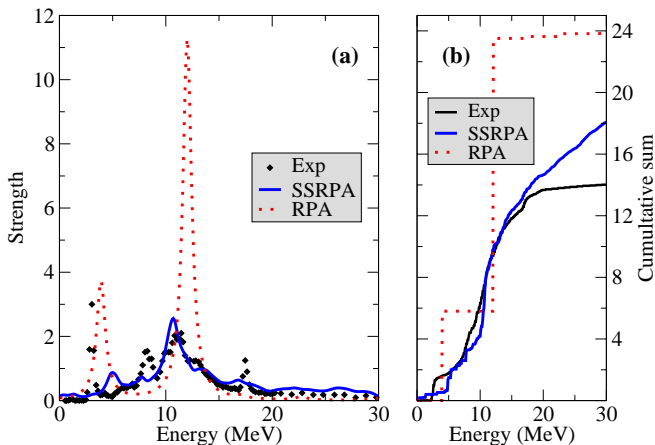


Figure 2. (a)  $GT^-$  strength distributions in  $\text{MeV}^{-1}$ . The experimental points are extracted from Ref. [55]. The RPA and SSRPA responses, computed with the parameterization SGII, are folded with a Lorentzian having a width of 1 MeV. (b) Cumulative strengths up to 30 MeV.

Figure 1 shows the experimental strength extracted from Ref. [55]. One of the most important features of the SSRPA is its ability to describe the width and fragmentation of excitation spectra. This asset is visible in the figure, which contains both the RPA and SSRPA discrete-strength distributions. Because the experimental strength is a continuous function of energy, it has different units from the discrete theoretical strengths, and the absolute strength values are thus not comparable. However, by plotting the discrete spectra one can compare the location and fragmentation of the main peaks, without generating any artificial spreading by folding. To better display the results in the figure, we rescale the RPA and SSRPA discrete strengths so that their respective highest peaks have approximately the same height as the corresponding experimental peak. To achieve this, we divide the RPA strength by nine and multiply the SSRPA strength by two.

The SSRPA strength is indeed quite fragmented, particularly in the region between 6 and 16 MeV, where three groups of peaks are concentrated around 8, 11, and 14 MeV, in accordance with the experimental distribution of peaks. One may also observe another group of much weaker peaks concentrated around 17 MeV, which corresponds to the location of the highest-energy experimental peak. Finally, a very dense high-energy SSRPA tail is visible in the insert, which focuses on the energy region between 20 and 30 MeV. Such a tail is completely absent from the RPA spectrum, which is composed of a few well separated peaks and misses the complex structure of the experimental strength. The long high-energy tail is indeed the explanation for the missing strength at lower energies.

The very lowest-energy part of the SSRPA spectrum is less satisfactory than the rest, with a main peak predicted at about 5 MeV; the lowest experimental peak,

by contrast, is located at 3 MeV. The SSRPA does predict some fragmented strength is in the region around 3 MeV, however. The RPA discrete spectrum in Fig. 1, by contrast, shows only a single visible peak at 4 MeV.

To more directly compare the theoretical and experimental strengths, we have folded our response functions together with a Lorentzian distribution of width 1 MeV. Panel (a) of Fig. 2 presents the folded RPA and SSRPA strength distributions along with the experimental distribution. Panel (b) shows the cumulative strength as a function of energy up to 30 MeV. As we have already seen in the discrete spectra, the SSRPA reproduces the GT distribution quite well, with the exception of the lowest-energy peak. The RPA, on the other hand, cannot reproduce the complex structure of the spectrum.

The most striking result is in panel (b). The SSRPA cumulative strength is greatly reduced from that of the RPA and is in much better agreement with the experimental value, even at low energies. Furthermore, the SSRPA curve is smooth and follows the experimental profile (owing to the physical description of widths and fragmentation, and to the subtraction procedure, which is needed to place centroids at the correct energies), except beyond 20 MeV, where the tail is a little too high. The RPA curve, by contrast, shows steps because of its very few well separated peaks. The improvement with respect to the RPA is more significant than in other beyond-mean-field approaches. In Ref. [37], for example, the same Skyrme interaction SGII produces more than 20 units of strength below 20 MeV.

The ratio between the experimental and the theoretical integrated strength below 20 MeV is 0.58 for the RPA and 0.93 for the SSRPA, showing that quenching factors are not needed in SSRPA. In the particle-vibration-coupling calculations of Ref. [37], this ratio is  $\leq 0.68$ , with the upper limit corresponding to an integrated strength of 20 units. The explicit inclusion of 2p2h configurations efficiently generates the high-energy tail that accounts for the missing strength. When we integrate the strength up to 70 MeV, we obtain a total of 23.84. The integrated  $\beta^+$  strength at that energy is only 0.10, so we reproduce the Ikeda sum of 24 to within about 1%.

To generalize our analysis, and to show that the decrease in strength below 20 MeV is an intrinsic effect of the SSRPA and not an artifact of a specific parameterization, we show in Fig. 3 RPA and SSRPA results obtained with three different parameterizations — SGII, SkM\* [56], and SkMP [57] — together with their experimental counterparts. Panels (a), (b), and (c) show the cumulative strengths up to 20 MeV, whereas panel (d) displays the percentages of the Ikeda sum rule from strength below 30 MeV. For this last quantity, Ref. [55] has reported both the experimental value and its uncertainty. In all three upper panels the integrated strength in the SSRPA is smaller than in the RPA, especially for SGII and SkM\*. With these two parameterizations, the percentages of the Ikeda sum in panel (d) are quite close to the experimental value. The upper panels show that

the detailed structure of the experimental spectrum is best reproduced by the parameterization SGII; in panel (a) the curve follows the experimental profile very closely.

We turn now to  $^{78}\text{Ni}$ . Though the GT spectrum of this nucleus has never been measured, its  $\beta$ -decay lifetime is known [58]. Our GT $^-$  strength, integrated up to 20 MeV, appears in Fig. 4(a) from both the RPA and SSRPA (this time in a diagonal approximation so that we can invert the larger  $A_{22}$  in this heavier nucleus). The figure also displays two other theoretical values for the integrated strength at 20 MeV, from the beyond-mean-field calculations of Refs. [35] and [59] (for the latter, with the same interaction SGII as we use). Our value is significantly lower than those of both the RPA and the other two beyond-mean-field calculations.

Finally, we use our computed GT strength to obtain the  $\beta$ -decay half-life of  $^{78}\text{Ni}$ . Because correlations make *ad-hoc* quenching unnecessary in our approach, we use the bare value 1.28 for  $g_A$ , the weak axial-vector coupling constant. Our result appears in Fig. 4(b), together with the experimental value [58]. The SSRPA half-life is 0.19 seconds, very close to the experimental half-life. The RPA half-life, by contrast, is 9.51 seconds with the bare value of  $g_A$ . The predictions of Refs. [35] (in the most complete scheme that includes polarization effects related to CE phonons) and [59] (with the interaction SGII) are 0.04 and 0.69 seconds respectively, again without  $g_A$  renormalization. Both these results are farther from the experimental half-life than ours.

In summary, we have presented a crucial improve-

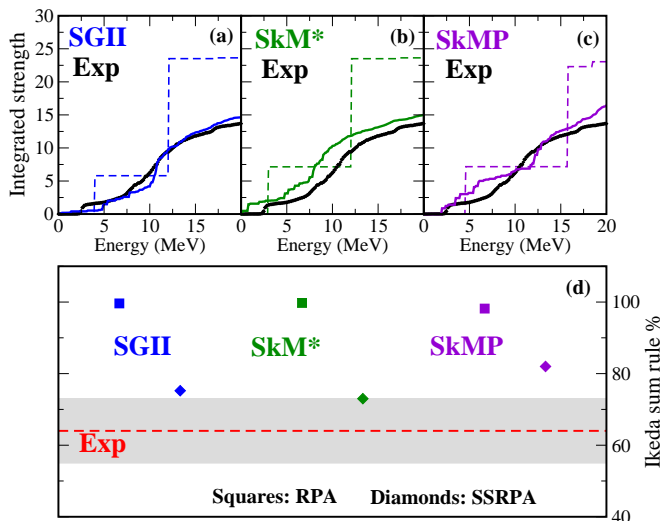


Figure 3. (a), (b), (c) Strengths integrated up to 20 MeV. The black symbols represent the experimental values [55]. The solid (dashed) lines correspond to the SSRPA (RPA) results obtained with the parameterizations SGII (a), SkM\* (b), and SkMP (c). (d) Experimental percentage of the Ikeda sum rule below 30 MeV extracted from Ref. [55] (red dashed horizontal line), and its associated uncertainty (grey area). RPA and SSRPA percentages obtained with the parameterizations SGII, SkM\*, and SkMP are also shown.

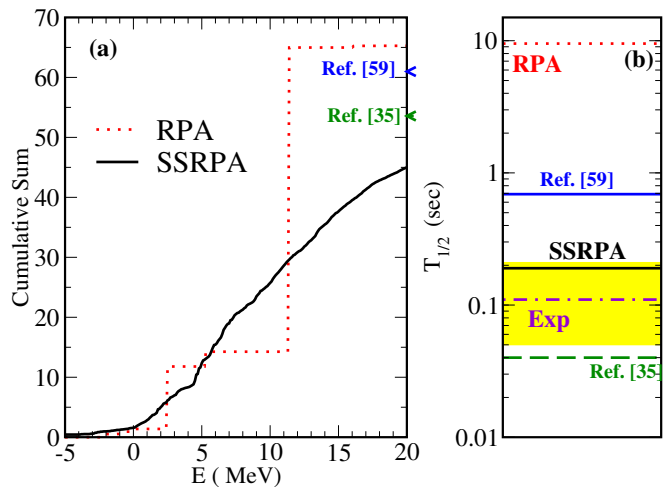


Figure 4. (a) Cumulative sum for different models (see legend and text) for the nucleus  $^{78}\text{Ni}$ ; (b)  $\beta$ -decay half-life for  $^{78}\text{Ni}$  predicted by SSRPA, compared with predictions of other models and the experimental value [58]. The yellow band represents the experimental uncertainty.

ment in the description of the GT strength for the lightest double- $\beta$  emitter, the nucleus  $^{48}\text{Ca}$ , and the heavier nucleus  $^{78}\text{Ni}$ . This achievement was made possible by the beyond-mean-field EDF-based CE-SSRPA, developed here for the first time. We have used the approach to compute GT $^-$  strengths with the Skyrme interaction SGII, and shown that it reproduces the complex fragmented spectrum in  $^{48}\text{Ca}$  much better than does the RPA. Our most important result is that the total SSRPA strength below 20-30 MeV is much smaller than in other mean-field and beyond-mean-field EDF models, and in better agreement with the corresponding experimental values, without the use of *ad hoc* quenching factors. By working with two additional Skyrme parameterizations we showed that these successes are due primarily to our many-body method, the key ingredient of which is the explicit inclusion of 2p2h configurations. Their density strongly increases with the excitation energy, leading to a high-energy tail in the spectrum. We showed that the same effects reduce the GT strength in the nucleus  $^{78}\text{Ni}$ , so that the predicted  $\beta$ -decay half-life agrees better with experiment than do other beyond-mean-field models.

The ability to describe CE strength may have a strong impact in astrophysical scenarios where GT resonances play an important role. It also promises to improve EDF-based calculations of the nuclear matrix elements governing  $0\nu\beta\beta$  decay, a process at the intersection of several scientific domains. Our less accurate reproduction of the weak low-energy part of the  $^{48}\text{Ca}$  spectrum is unlikely to have a large effect on the  $0\nu\beta\beta$  matrix element, which contains an unweighted sum over states at all energies. We plan to apply our approach to open-shell nuclei by including pairing correlations of both the usual isovector type and the isoscalar type that are important for  $\beta$  and double- $\beta$  decay [26, 60–62].

## ACKNOWLEDGMENTS

M.G. acknowledges funding from the European Union Horizon 2020 research and innovation program under

Grant No. 654002 and from the IN2P3-CNRS BRIDGE-EDF project. J.E. acknowledges support from the U.S. Department of Energy (DOE), Office of Science, under Grant No. DE-FG02-97ER41019.

- 
- [1] F. Osterfeld, *Rev. Mod. Phys.* **64**, 491 (1992).
- [2] M. Ichimura, H. Sakai, and T. Wakasa, *Prog. Part. Nucl. Phys.* **56**, 446 (2006).
- [3] K. Langanke and G. Martínez-Pinedo, *Rev. Mod. Phys.* **75**, 819 (2003).
- [4] H.-T. Janka, K. Langanke, A. Marek, G. Martínez-Pinedo, and B. Müller, *Physics Reports* **442**, 38 (2007), the Hans Bethe Centennial Volume 1906-2006.
- [5] F. T. Avignone, S. R. Elliott, and J. Engel, *Rev. Mod. Phys.* **80**, 481 (2008).
- [6] J. Engel and J. Menéndez, *Reports on Progress in Physics* **80**, 046301 (2017).
- [7] J. Menéndez, *Journal of Physics G: Nuclear and Particle Physics* **45**, 014003 (2017).
- [8] N. Shimizu, J. Menéndez, and K. Yako, *Phys. Rev. Lett.* **120**, 142502 (2018).
- [9] E. Santopinto, H. García-Tecocoatzi, R. I. Magaña Vsevolodovna, and J. Ferretti (NUMEN Collaboration), Heavy-ion double-charge-exchange and its relation to neutrinoless double- $\beta$  decay, *Phys. Rev. C* **98**, 061601 (2018).
- [10] V. d. S. Ferreira, A. R. Samana, F. Krmpotić, and M. Chiapparini, Nuclear structure model for double-charge-exchange processes, *Phys. Rev. C* **101**, 044314 (2020).
- [11] F. Cappuzzello et al., *Eur. Phys. J. A* **54**, 72 (2018).
- [12] H. Lenske, F. Cappuzzello, M. Cavallaro, and M. Colonna, *Prog. Part. Nucl. Phys.* **109**, 103716 (2019).
- [13] J. M. Yao, B. Bally, J. Engel, R. Wirth, T. R. Rodríguez, and H. Hergert, *Phys. Rev. Lett.* **124**, 232501 (2020).
- [14] S. J. Novario, P. Gysbers, J. Engel, G. Hagen, G. R. Jansen, T. D. Morris, P. Navrátil, T. Papenbrock, and S. Quaglioni, Coupled-cluster calculations of neutrinoless double-beta decay in  $^{48}\text{Ca}$  (2020), arXiv:2008.09696 [nucl-th].
- [15] A. Bellei, C. G. Payne, S. R. Stroberg, T. Miyagi, and J. D. Holt, Ab initio neutrinoless double-beta decay matrix elements for  $^{48}\text{Ca}$ ,  $^{76}\text{Ge}$ , and  $^{82}\text{Se}$  (2020), arXiv:2008.06588 [nucl-th].
- [16] J. Menéndez, A. Poves, E. Caurier, and F. Nowacki, *Nucl. Phys. A* **818**, 139 (2009).
- [17] Y. Iwata, N. Shimizu, T. Otsuka, Y. Utsuno, J. Menéndez, M. Honma, and T. Abe, *Phys. Rev. Lett.* **116**, 112502 (2016), [Erratum: *Phys. Rev. Lett.* **117**, 179902 (2016)].
- [18] M. Horoi and A. Neacsu, *Phys. Rev. C* **93**, 024308 (2016).
- [19] J. Barea, J. Kotila, and F. Iachello, *Phys. Rev. C* **91**, 034304 (2015).
- [20] T. R. Rodríguez and G. Martínez-Pinedo, *Phys. Rev. Lett.* **105**, 252503 (2010).
- [21] N. L. Vaquero, T. R. Rodríguez, and J. L. Egido, *Phys. Rev. Lett.* **111**, 142501 (2013).
- [22] J. Yao, L. Song, K. Hagino, P. Ring, and J. Meng, *Phys. Rev. C* **91**, 024316 (2015).
- [23] J. Yao and J. Engel, *Phys. Rev. C* **94**, 014306 (2016).
- [24] F. Šimković, V. Rodin, A. Faessler, and P. Vogel, *Phys. Rev. C* **87**, 045501 (2013).
- [25] J. Hyvriinen and J. Suhonen, *Phys. Rev. C* **91**, 024613 (2015).
- [26] M. Mustonen and J. Engel, *Phys. Rev. C* **87**, 064302 (2013).
- [27] L.-G. Cao, S.-S. Zhang, and H. Sagawa, *Phys. Rev. C* **100**, 054324 (2019).
- [28] A. Bohr and B. R. Mottelson, On the role of the  $\delta$  resonance in the effective spin-dependent moments of nuclei, *Physics Letters B* **100**, 10 (1981).
- [29] G. Bertsch and I. Hamamoto, *Phys. Rev. C* **26**, 1323 (1982).
- [30] S. Ait-Tahar and D. Brink, *Nucl. Phys. A* **560**, 765 (1993).
- [31] A. Klein, W. G. Love, and N. Auerbach, Continuum charge-exchange spectra and the quenching of gamow-teller strength, *Phys. Rev. C* **31**, 710 (1985).
- [32] P. Gysbers et al., *Nature Phys.* **15**, 428 (2019).
- [33] A. Ekström, G. R. Jansen, K. A. Wendt, G. Hagen, T. Papenbrock, S. Bacca, B. Carlsson, and D. Gazit, *Phys. Rev. Lett.* **113**, 262504 (2014).
- [34] L. Coraggio, L. De Angelis, T. Fukui, A. Gargano, N. Itaco, and F. Nowacki, *Phys. Rev. C* **100**, 014316 (2019).
- [35] C. Robin and E. Litvinova, *Phys. Rev. C* **98**, 051301 (2018).
- [36] C. Robin and E. Litvinova, *Phys. Rev. Lett.* **123**, 202501 (2019).
- [37] Y. F. Niu, G. Colò, and E. Vigezzi, *Phys. Rev. C* **90**, 054328 (2014).
- [38] D. Gambacurta and F. Catara, Collective excitations in metallic clusters within the second random phase approximation, *Journal of Physics: Conference Series* **168**, 012012 (2009).
- [39] D. Peng, Y. Yang, P. Zhang, and W. Yang, Restricted second random phase approximations and tamm-dancoff approximations for electronic excitation energy calculations, *The Journal of Chemical Physics* **141**, 214102 (2014).
- [40] N. Auerbach, A. Klein, and N. Van Giai, The giant dipole resonance and its charge-exchange analogs, *Physics Letters B* **106**, 347 (1981).
- [41] N. Auerbach, L. Zamick, and A. Klein, Rpa calculations of isovector spin-flip excitations, *Physics Letters B* **118**, 256 (1982).
- [42] A. Lane and J. Martorell, The random phase approximation: Its role in restoring symmetries lacking in the hartree-fock approximation, *Annals of Physics* **129**, 273 (1980).
- [43] V. Tselyaev, *Phys. Rev. C* **88**, 054301 (2013).
- [44] D. Gambacurta, M. Grasso, and J. Engel, *Phys. Rev. C* **92**, 034303 (2015).
- [45] D. Gambacurta, M. Grasso, and O. Vasseur, *Phys. Lett. B* **777**, 163 (2018).
- [46] O. Vasseur, D. Gambacurta, and M. Grasso, *Phys. Rev.*

- C **98**, 044313 (2018).
- [47] M. Grasso, D. Gambacurta, and O. Vasseur, Phys. Rev. C **98**, 051303 (2018).
- [48] D. Gambacurta, M. Grasso, and O. Sorlin, Phys. Rev. C **100**, 014317 (2019).
- [49] M. Grasso and D. Gambacurta, Phys. Rev. C **101**, 064314 (2020).
- [50] T. Skyrme, Phil. Mag. **1**, 1043 (1956).
- [51] T. Skyrme, Nucl. Phys. **9**, 615 (1959).
- [52] D. Vautherin and D. Brink, Phys. Rev. C **5**, 626 (1972).
- [53] N. van Giai and H. Sagawa, Phys. Lett. B **106**, 379 (1981).
- [54] N. V. Giai and H. Sagawa, Nuclear Physics A **371**, 1 (1981).
- [55] K. Yako et al., Phys. Rev. Lett. **103**, 012503 (2009).
- [56] J. Bartel, P. Quentin, M. Brack, C. Guet, and H.-B. Hakansson, Nucl. Phys. A **386**, 79 (1982).
- [57] L. Bennour, P.-H. Heenen, P. Bonche, J. Dobaczewski, and H. Flocard, Phys. Rev. C **40**, 2834 (1989).
- [58] P. T. Hosmer, H. Schatz, A. Aprahamian, O. Arndt, R. R. C. Clement, A. Estrade, K.-L. Kratz, S. N. Liddick, P. F. Mantica, W. F. Mueller, F. Montes, A. C. Morton, M. Ouellette, E. Pellegrini, B. Pfeiffer, P. Reeder, P. Santi, M. Steiner, A. Stolz, B. E. Tomlin, W. B. Walters, and A. Wöhr, Half-life of the doubly magic  $r$ -process nucleus  $^{78}\text{Ni}$ , Phys. Rev. Lett. **94**, 112501 (2005).
- [59] Y. F. Niu, Z. M. Niu, G. Colò, and E. Vigezzi, Particle-vibration coupling effect on the  $\beta$  decay of magic nuclei, Phys. Rev. Lett. **114**, 142501 (2015).
- [60] M. Mustonen, T. Shafer, Z. Zenginerler, and J. Engel, Phys. Rev. C **90**, 024308 (2014).
- [61] C. Bai, H. Sagawa, G. Col, Y. Fujita, H. Zhang, X. Zhang, and F. Xu, Phys. Rev. C **90**, 054335 (2014).
- [62] Y. Niu, G. Colo, E. Vigezzi, C. Bai, and H. Sagawa, Phys. Rev. C **94**, 064328 (2016).